Volume 1 | Number 1 | Jan 2013 | Pages 1–100

Nanoscale

www.rsc.org/nanoscale

ROYAL SOCIETY OF CHEMISTRY

This is an *Accepted Manuscript*, which has been through the Royal Society of Chemistry peer review process and has been accepted for publication.

Accepted Manuscripts are published online shortly after acceptance, before technical editing, formatting and proof reading. Using this free service, authors can make their results available to the community, in citable form, before we publish the edited article. We will replace this *Accepted Manuscript* with the edited and formatted *Advance Article* as soon as it is available.

You can find more information about *Accepted Manuscripts* in the **Information for Authors**.

Please note that technical editing may introduce minor changes to the text and/or graphics, which may alter content. The journal's standard **Terms & Conditions** and the **Ethical guidelines** still apply. In no event shall the Royal Society of Chemistry be held responsible for any errors or omissions in this *Accepted Manuscript* or any consequences arising from the use of any information it contains.

www.rsc.org/nanoscale

Journal Name

ARTICLE

Novel cobalt quantum dot/graphene nanocomposites as highly efficient electrocatalysts for water splitting

Maduraiveeran Govindhan, Brennan Mao and Aicheng Chen*

A cost-effective, non-noble metal based high-performance electrocatalyst for the oxygen evolution reaction (OER) is critical to energy conversion and storage processes. Here, we report on a facile and effective in situ strategy for the synthesis of an advanced nanocomposite material that is comprised of cobalt quantum dots (Co QDs, ~3.2 nm), uniformly dispersed on reduced graphene oxide (rGO) as a highly efficient OER electrocatalyst platform. This nanocomposite electrocatalyst afforded a mass activity of 1250 A g^{-1} at a low overpotential (η) of 0.37 V, a small Tafel slope of ~37 mV dec^{-1} and a turnover frequency (TOF) of 0.188 s^{-1} in 0.1 M KOH, comparing favorably with state-of-the-art RuO_2, IrO_2 and Pt/C catalysts. The synergy between abundant catalytically active sites through the fine dispersion of Co QDs, and enhanced electron transfer generated from the graphene resulted in the first-rate electrocatalytic properties toward the OER. These merits coupled with the higher stability of the nanocomposite hold great promise for triggering breakthroughs in electrocatalysis for water splitting.

Introduction

The growing demand for sustainable energy coupled with increasing environmental concerns has stimulated intense research in energy conversion and storage systems with low cost, high efficiency and environmental compatibility.[1] The splitting of water into hydrogen and oxygen is one of the most important, albeit challenging, electrochemically/ photoelectrochemically driven chemical energy conversion processes.[2] One of the key issues in water splitting is the oxygen evolution reaction (OER) at the anode. However, OER involves a complex four-electron oxidation process, where sluggish kinetics can result in considerable electrochemical overpotential (η) requirements that lead to substantial losses to overall water splitting efficiencies.[3] A several hundred millivolt overpotential is often vital in achieving a current density of 10 A g^{-1}.[4] Therefore, the development of an effective electrocatalyst is required to accelerate the reaction while reducing the large overpotential to thus improve the energy conversion efficiency. Commercially available water electrolysis systems rely on ruthenium (Ru), iridium (Ir), platinum (Pt), ruthenium oxide (RuO_2) and iridium oxide (IrO_2) catalysts; however, these materials are expensive and have limited availability.[5] The discovery of alternative, robust, and efficient catalysts that are abundantly available, and have equivalent catalytic activity and durability for OER are highly desirable for the development of viable water electrolytic systems. In recent years, many metal oxides have been intensively studied as potential OER catalysts to replace Pt, Ru

and Ir based metals.[6] Recent research has led to the emergence of cobalt (Co) as a relatively promising candidate for OER via photocatalytic and electrocatalytic processes due to its low cost, abundance, thermal stability, and environmental compatibility.[2,6,7] Besides being plentiful and economical, Co based materials enable water oxidation with moderate overpotentials under alkaline conditions.[8] However, Co based materials still exhibit relatively low catalytic activity with limited large-scale applications when compared to noble metals-based OER catalysts, due to poor electrical conductivity and a limited number of active sites.[9] Considerable efforts have been made toward the design of efficient electrocatalysts that exhibit highly dense surface resident reactive sites, thus facilitating a far greater cumulative available area for contact with reactants and resulting in enhanced catalytic activity toward OER. The activity of OER electrocatalysts may be further improved at the nanoscale through the modification of their surfaces by tuning their composition.[10] Moreover, the synergistic chemical coupling effects between Co catalysts and selected substrates are believed to contribute to a significant performance enhancement.[11]

Graphene is a two-dimensional (2D) single carbon atom thick monolayer that comprises a desirable matrix for the support of non-precious metals/metal oxides, which has strong potential in the development of advanced materials for electrocatalysis and other energy-related applications.[12-14] The morphology and electrical conductivity of catalysts affect electrocatalytic efficiency, thus the use of carbon substrates improves the conductivity of composite catalysts while increasing the dispersion of reactive sites.[15,16] A survey of the literature reveals that, to date, Co based oxide/graphene composites for OER have relatively larger CoO_x dimensions

Department of Chemistry, Lakehead University, 955 Oliver Road, Thunder Bay, ON P7B 5E1, Canada. E-mail: achen@lakeheadu.ca

(>10 nm up to hundreds of nanometers), involve complicated processes, have unsatisfactory dispersions, and require high hydrothermal temperatures and elongation timelines.[17,18]

The growth of highly dispersible nanometric metal and metal oxides on graphene may enable efficient performance via the establishment of robust chemical and electrical coupling, as well as the potential development of optimized electronic structures.[19] Herein, we report on the synthesis of a monodisperse (~3.2 nm) Co QD/graphene nanocomposite that exhibited high OER electrocatalytic performance with a low overpotential and a small Tafel slope, which compared favorably with some benchmarking catalysts, and was highly stable in 0.1M KOH. Our experimental results have shown that the synthesized Co QD/graphene nanocomposite with a large number of active sites is a strong candidate for expediting OER.

Experimental section

Materials

GO (2 mg/mL), cobalt(II) sulfate heptahydrate, sodium borohydride, potassium hydroxide and a 10 wt.% Nafion solution were purchased from Sigma-Aldrich. All other analytical grade reagents were used as received. Pure water produced with a NANOpure® water system was utilized in the preparation of all solutions. All electrochemical experiments were carried out in 0.1 M KOH (~pH 13) electrolyte solutions.

Synthesis of Co QD/rGO Nanocomposite

The Co QD/rGO nanocomposite was prepared in water via a facile chemical method at room temperature. In a typical synthesis, 1 mg/mL of GO was dispersed in 5 mL water. Subsequently, 2 mM concentration of cobalt (II) sulfate heptahydrate was added directly into the GO solution and magnetically stirred at 1250 rpm (Thermo Scientific) for 5 min. Ar-gas was employed to purge the solution for 20 min. Subsequently, 5 mM sodium borohydride was added to the mixture under vigorous stirring for 30 min in an Ar-environment, and the final solution was aged for 12 h under an Ar-atmosphere at room temperature (20±2°C). The preparation of the Co QD/rGO nanocomposite was used as the molar ratio of Co^{2+} and sodium borohydride (2:5). For comparison, Co nanoparticles were prepared by a chemical reduction method under similar experimental conditions. Cobalt (II) sulfate heptahydrate (2 mM) was dispersed in 5 mL water under vigorous magnetic stirring in the absence of GO. Sodium borohydride (5 mM) was then added to the Co ion solution and stirred for 30 min and aged for 12 h. The preparation of Co and Co QD/rGO nanocomposite was carried out under Ar-environmental conditions.

Materials Characterization

The synthesized nanomaterials were characterized by various analytic techniques. Morphological surface studies, energy dispersive X-ray spectroscopy (EDX) and elemental mapping were performed utilizing a field emission scanning electron microscope (FE-SEM) (Hitachi SU-70). Transmission electron microscopic (TEM) measurements were performed by JEOL 2010F TEM with a resolution of 0.23 nm. X-ray photoelectron spectra were recorded via a Thermo Fisher XPS system, where the size of the X-ray spot was 400 μm, using an Al Kα monochromatic source. X-ray diffraction (XRD) patterns were recorded using a Pananalytical Xpert Pro Diffractometer with Ni filtered monochromatic Cu Kr (1.5406 Å, 2.2 KW Max). The Fourier transform infrared (FTIR) spectra were recorded at room temperature with a Nicolet 8700 FT-IR spectrometer.

Electrochemical Measurements

Electrochemical experiments were performed with a CHI 660B electrochemical workstation (CH Instrument Inc. USA) utilizing a conventional one compartment three-electrode cell. A glassy carbon (GC) electrode (3 mm diameter, 0.07 cm^2) was employed as the working electrode, whereas a silver/silver chloride electrode (Ag/AgCl) was utilized as the reference electrode, and a platinum coil was used as the counter electrode. The GC electrode was polished (Microcloth, Buehler) using alumina powder (0.05 μm) followed by sonication in the pure water for 3 min and used as the electrode substrate. Argon (Ar) gas was introduced to purge the solution in achieving an O_2-free condition. All of the electrochemical experiments were performed at ambient room temperature (20 ± 2°C).

The fabrication procedure of the GC working electrodes modified with the investigated catalysts may be found as follows. The nanoscale Co QD/rGO composite catalyst was mixed with a 0.5% Nafion solution, whereafter the mixture was ultrasonicated for 10 min to generate a homogeneous ink. A known amount (5 μL) of Co QD/rGO composites was cast onto a GC electrode, leading to a catalyst loading of ~0.008 mg cm^{-2}. Finally, the catalyst film was air dried at room temperature. An identical loading of the Co catalyst was coated onto the GC electrode with the synthesized Co nanoparticles for comparison. To prepare the commercial Pt/C catalyst modified electrode, 4 mg of Pt/C catalyst (10wt% Pt) was dispersed in 1 mL of water with a 0.5wt % Nafion solution under 10 min of ultrasonication. The Pt/C catalyst ink (5 μL) was subsequently cast onto a GC electrode and dried at room temperature. The OER tests were performed in a 0.1 M KOH electrolyte, which was purged with high purity Ar for 20 min to remove all of the dissolved oxygen. Linear sweep voltammetry (LSV) curves were obtained by sweeping the electrode potential from 0 to 1.0 V vs Ag/AgCl at room temperature. All potentials measured in the present study against the Ag/AgCl electrode were converted to the reversible hydrogen electrode (RHE) scale on the basis of Nernst equation as follows:

$$E_{RHE} = E_{Ag/AgCl} + 0.059(pH) + 0.197 \text{ V} \qquad --------- (1)$$

Calculation Method

The overpotential (η) and Tafel slope were derived from the Tafel equation:[20]

$$\eta = b \log j + a \qquad --------- (2)$$

where j is the current density; b is the Tafel slope; and a is the constant.

　　　　　　　　　　　　　　　　　　　　　　　　　　　　　　　　　　　　　　　ARTICLE

Mass activity values (A g^{-1}) were calculated using the electrocatalyst loading m (g cm^{-2}) and the measured current density j (A cm^{-2}) at different overpotentials:

$$Mass\ activity = j / m \qquad --------- (3)$$

The turnover frequency (TOF) value was calculated by assuming that every metal atom is involved in the catalysis:[21]

$$TOF = (j \times S) / (4 \times F \times n) \qquad --------- (4)$$

Herein, j is the measured current density (10 mA cm^{-2}); S is the surface area of GC electrode; the number 4 is the number of electrons involved in OER; F is Faraday's constant; and n relates to the moles of metal atoms that are coated onto the electrode surface.

3. Results and Discussion

The formation of the Co QD/rGO nanocomposite was visually observed during the reduction of Co^{2+} and GO through changes in color, from light-yellow to dark-black. The morphology of the formed Co QD/rGO nanocomposite was characterized by FE-SEM. Fig. S1A and S1B (in the Electronic Supplementary Information) present the FE-SEM images of rGO and the Co QD/rGO nanocomposite, respectively. The ultrathin rGO sheets were observed in Fig. S1A; and tiny Co QDs were seen by close examination of the image displayed in Fig. S1B. Further characterization of the formed rGO and the Co QD/rGO nanocomposite was performed by TEM. Fig. 1A shows the low-resolution TEM image of nanocomposited graphene nanosheets with Co QDs. The HR-TEM image (Fig. 1B) displays that the average size of the formed Co QDs was estimated to be ~3.2 nm, which were homogeneously dispersed on the rGO sheets. Fig. 1C shows the selected area electron diffraction pattern of the Co QDs, the circles provide a set of diffraction of the (111), (200), (220) and (311) planes respectively of the face-centred cubic structure of Co.[22] For a further investigation of the Co QD/rGO nanocomposite, elemental mapping provided a meaningful illustration of the Co distribution in the composite materials (Fig. 1D). The elemental mapping result revealed that elemental Co was uniformly distributed on the rGO sheets, which is in good agreement with the SEM image (Fig. S1B). The XRD pattern of the Co QD/rGO nanocomposite is shown in Fig. S2, where the two sharp diffraction peaks (at 44.4° and 51.9°) indexed to the (111) and (200) reflections of the face-centered cubic (fcc) structure of metallic cobalt (JCPDS File No: 15-0806), are consistent with previous reports on metallic Co.[22,23] A weak and broadened diffraction peak at 26°, which might be ascribed to the (002) plane reflections of graphene.[24] All these XRD results indicate that the formed Co QD/rGO nanocomposite were comprised of well-crystallized Co and rGO.

The surface chemical compositions and the valence states of the Co QD/rGO nanocomposite were investigated by XPS. Fig. 2A and 2B display the C1s XPS of GO and rGO, respectively. The four peaks at 284.9, 286.2, 286.8 and 288.2 eV corresponded to sp^2 C, C–OH, C-O and C=O bonds, respectively,[25] revealing that the carbon species were highly
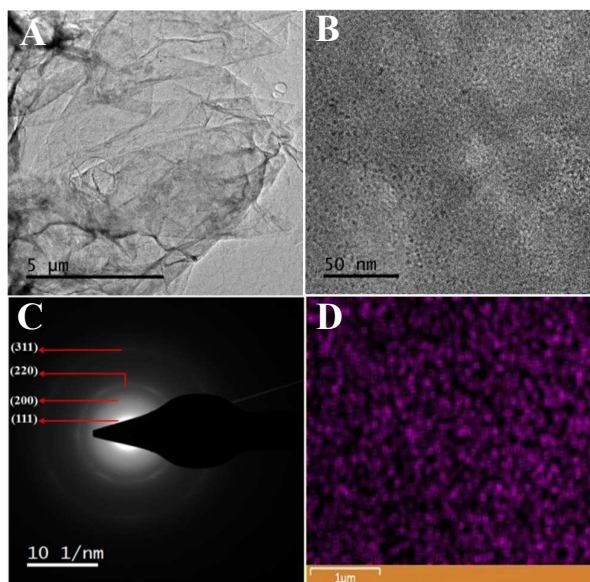
Fig. 1. TEM image (A), high-resolution TEM image (B) and the electronic diffraction pattern of the Co QD/rGO composites (C) and the EDX elemental mapping of Co in the Co QD/rGO nanocomposite (D).

oxidized in GO. In the case of rGO, a significant decrease of the intensities at the binding energies of 286.2 and 286.8 eV (C-OH and C-O) indicates the successful removal of exogenous functional groups through the chemical reduction. Fig. 2C reveals that the Co 2p XPS of the Co QD/rGO nanocomposite exhibited peaks at ~799.8 and 796.8 eV, corresponding to the Co $2p_{3/2}$ and Co $2p_{1/2}$ states, respectively. The obtained binding energies shifted to higher binding energies for Co $2p_{3/2}$ (799.8 eV) and Co $2p_{1/2}$ (796.8 eV) as compared to metallic Co (Co $2p_{3/2}$ (778.1 eV) and Co $2p_{1/2}$ (793.3 eV), indicating that the Co on the surface of the rGO sheets was being partially oxidized.[23] Fig. S3 shows the FTIR spectra recorded for the GO, rGO and Co QD/rGO nanocomposite. The IR spectrum of GO shows the bands at broad 3400 cm^{-1} (υ(-OH)), 1730 cm^{-1} (υ(C=O)) and 1003 cm^{-1} (υ(C=C)), respectively. Upon the reduction of GO to rGO, υ(-OH) and υ(C=O) bands disappeared, further confirming the removal of oxygen functional groups from GO.
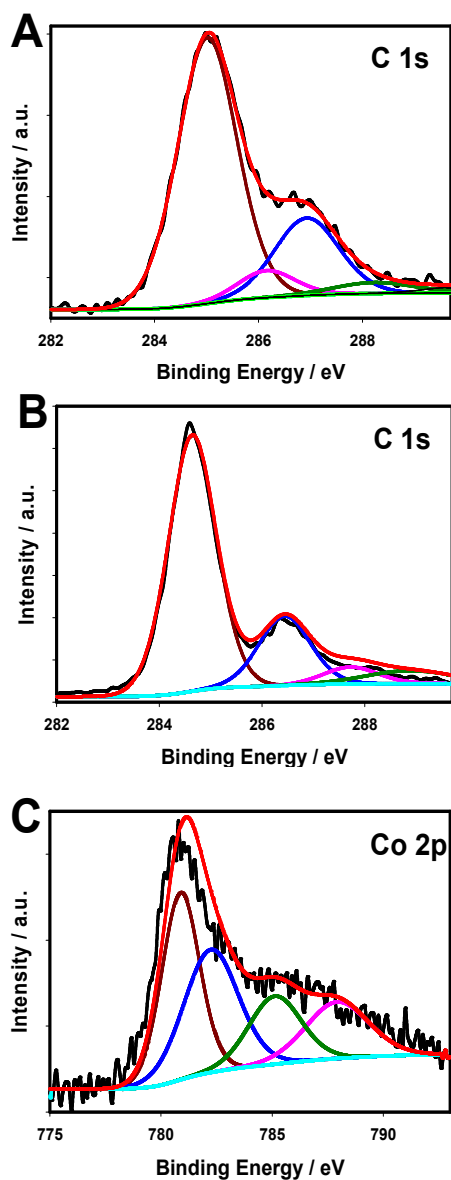
Fig. 2. XPS obtained for the synthesized GO (A) and Co QD/rGO nanocomposite (B and C).

The electrocatalytic activity of the Co QD/rGO nanocomposite was investigated with respect to OER in 0.1 M KOH. The Co QD/rGO nanocomposite was uniformly coated on a GC substrate and used as the working electrode. In the present investigation, similar experimental measurements were also carried out with other electrodes for comparison including commercial Pt/C and Co nanoparticle catalysts. Linear sweep voltammograms (LSVs) (Fig. 3) were recorded for OER with various electrodes, including a bare GC electrode as well as the GC electrodes modified with rGO, Co, Pt/C, and the Co QD/rGO nanocomposite, respectively. As expected, no obvious current responses were obtained at the bare GC and the rGO modified GC electrodes (Inset of Fig. 3). The dispersion of Co QDs on rGO sheets exhibited efficient OER catalytic

current densities in contrast to all other electrodes included in this investigation, as shown in Fig. 3. The Co QD/rGO nanocomposite electrode possessed a high electrocatalytic current density of 32.13 mA cm^{-2} at 1.86 V in 0.1 M KOH, which was 6.45 and 3.63 times larger than that of the GC electrode modified with the Co nanoparticles (4.94 mA cm^{-2}) and the commercial state-of-the-art Pt/C (8.84 mA cm^{-2}), respectively. Fig. S4 displays the plots of the OER onset potential and oxidation potential (at 5 mA cm^{-2}) of the Co, commercial Pt/C and the Co QD/rGO modified GC electrodes. Both the Co QD/rGO nanocomposite and the Pt/C exhibited a similar onset potential (1.43 V vs RHE), which is much lower than that of the GC electrode modified with the Co nanoparticles (1.57 V). The overpotential measured of the Co, commercial Pt/C and the Co QD/rGO modified GC electrodes measured at 5 mA cm^{-2} was decreased in the in the following order: 1.83 > 1.68 > 1.57 V, further confirming that the Co QD/rGO nanocomposite possessed higher catalytic activity than the state-of-the-art Pt/C.
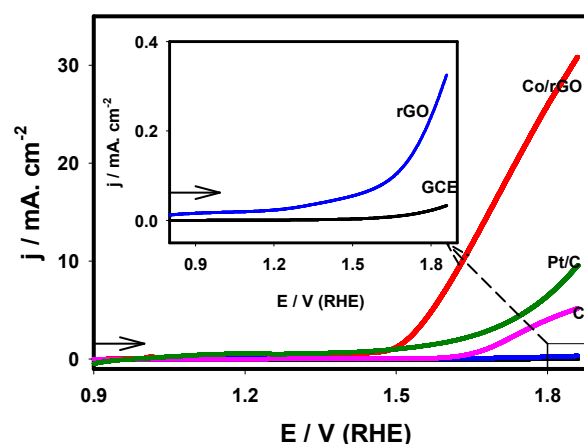
Fig. 3. LSV curves for OER at the bare GC electrode and the modified GC electrodes comprised of the Co QD/rGO composite, Co and commercial Pt/C. **Inset**: LSV curves for OER at the bare GC and GC electrode modified with rGO. Electrolyte: 0.1M KOH; Scan rate: 20 mV s^{-1}.

Electrochemical impedance spectroscopic (EIS) measurements were employed to further investigate the OER activity of the synthesized Co QD/rGO nanocomposite. Fig. 4 presents Nyquist impedance plots of the bare GC electrode and the GC electrodes modified with rGO and the Co QD/rGO nanocomposite in 0.1 M KOH at the applied potentials of 1.56 V (Fig. 4A), 1.66 V (Fig. 4B) and 1.76 V (Fig. 4C). These EIS results were fitted with the equivalent electric circuit presented in the inset of Fig. 4A. In this equivalent electric circuit, R_s represents the uncompensated solution resistance, R_p is the polarization resistance and the constant phase element (CPE) which is defined by CPE-T and CPE-P. The fitting curves are presented in the solid lines together with the experimental data (indicated as symbols), and are shown in

ARTICLE
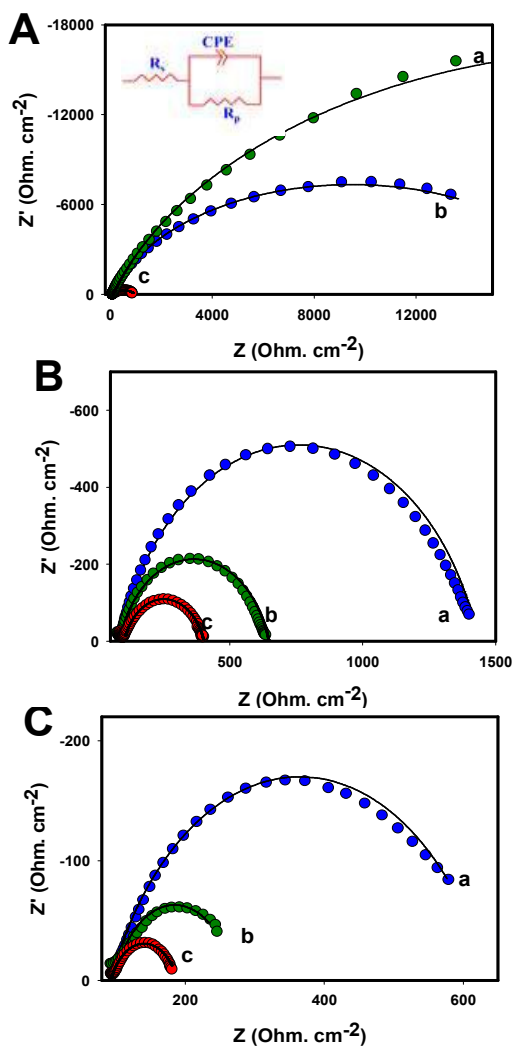
Fig. 4. Nyquist plots of a bare GC electrode (a) and the GC electrodes modified with the rGO (b) and the Co QD/rGO nanocomposite (c) recorded at the applied potential of 1.56 (A), 1.66 (B) and 1.76 V (C) in 0.1M KOH. The amplitude of modulation potential was 5 mV. The frequency was altered, from 100 kHz to 40 mHz. The inset of Fig. 4A is the corresponding equivalent electric circuit.

Fig. 4. These values, along with the errors (%) obtained via the fitting of the experimental data, are summarized in Table 1. All the fitting errors were less than 5%, indicating that the proposed equivalent electric circuit is effective for fitting the impedance data. The R_s values found for all of the electrodes were in the range of 82.9 - 119 Ω cm^2 under different applied potentials. The polarization resistance (R_p) was contingent on the applied electrode potential, and the R_p value for the Co QD/rGO nanocomposite electrode is much smaller than that of other electrodes presented in this investigation at all applied electrode potentials. The R_p values were decreased from 0.85 to 0.18 kΩ cm^2 by increasing the applied electrode potential from 1.56 to 1.76V, as illustrated in Table 1. The CPE-P values

are around 0.8, suggesting that the CPE-T values obtained in this study are close to the double-layer capacitance (C_{dl}). The CPE-T values of the Co QD/rGO nanocomposite electrode are 135, 180.8 and 247.2 µF cm^{-2} under the applied electrode potentials of 1.56, 1.66 and 1.76V, respectively. The Co QD/rGO nanocomposite electrode showed larger CPE-T values than the rGO modified and bare GC electrodes (Table 1). All the EIS results show that the Co QD/rGO nanocomposite electrode possessed a much higher charge-transfer rate between the electrolyte and the active material, which is consistent well with the LSV results, as displayed in Fig. 3.

Table 1. EIS data obtained from Nyquist plots of Fig. 4 (numbers in parentheses present the error as a percentage).

E/V	Electrodes	Rs [Ω cm^2]		R_p [k.Ω cm^2]		CPE-T [µF.cm^2]		CPE-P	
	GCE	85.0	(1.5)	41.7	(2.3)	72.4	(2.5)	0.8	(0.5)
1.56	rGO	82.9	(1.1)	18.8	(2.6)	79.7	(2.5)	0.8	(0.5)
	Co QD/rGO	87.7	(0.7)	0.8	(0.7)	135.0	(2.4)	0.9	(0.7)
	GCE	85.5	(1.3)	1.3	(1.9)	72.3	(1.3)	0.8	(1.0)
1.66	rGO	84.2	(1.2)	0.5	(1.8)	90.9	(3.8)	0.8	(1.4)
	Co QD/rGO	83.1	(4.1)	0.3	(1.9)	188.8	(1.9)	0.8	(1.8)
	GCE	92.6	(1.7)	0.6	(2.9)	147.0	(2.4)	0.8	(2.1)
1.76	rGO	119.0	(0.9)	0.3	(1.8)	183.4	(1.2)	0.8	(1.7)
	Co QD/rGO	100.4	(0.9)	0.1	(1.7)	247.2	(3.5)	0.8	(2.5)

The OER activity of the Co QD/rGO nanocomposite was further investigated using the chronopotentiometric and amperometric methods, as shown in Fig. 5A and 5B. For comparison, the electrocatalytic activity of the GC electrode modified with Co nanoparticles was also examined, and the obtained results are presented in Fig. S5. Fig. 5A displays three plots of the electrode potential (E) versus time (t) under the applied current densities of 5, 10 and 20 mA cm^{-2}. The corresponding electrode potential measured at t = 60 s was 1.53, 1.68 and 1.80 V, respectively, which was approximately 400 mV lower than that of the GC electrode modified with Co nanoparticles under the same applied current densities as seen in Fig. S5A. The effect of the applied potential on the measured current was also studied; Fig. 5B presents three curves of the current density (j) versus t under the applied electrode potentials of 1.56, 1.66 and 1.76 V. The corresponding steady-state current densities measured at t = 60 s were 4.07, 10.38 and 16.28 mA cm^{-2}, respectively, which were approximately 10 times higher than that of the GC electrode modified with Co nanoparticles under the same applied electrode potential as shown in Fig. S5B. The OER kinetics of the Co QD/rGO nanocomposite was probed by corresponding Tafel plots, as shown in Fig. 5C. The resulting Tafel slopes were found to be 260, 120 and 37 mV dec^{-1} for the rGO, Co and Co QD/rGO nanocomposite, respectively, showing that the Co QD/rGO nanocomposite catalyst exhibited the smallest Tafel slope, and was therefore the most efficient electrocatalyst among the studied electrocatalyst materials for OER. Comparison of the mass activity, overpotential, Tafel slope and turnover frequency of the new Co QD/rGO nanocomposite synthesized in the present study with the high-

performance OER electrocatalysts in alkaline solution recently reported in the literature is presented in Table 2. It is well-known that a smaller Tafel slope is more beneficial for water splitting applications, since it can offer an increased OER rate with a decrease of overpotential. It is worth mentioning that the Tafel slope of 37 mV dec^{-1} for the Co QD/rGO catalyst is
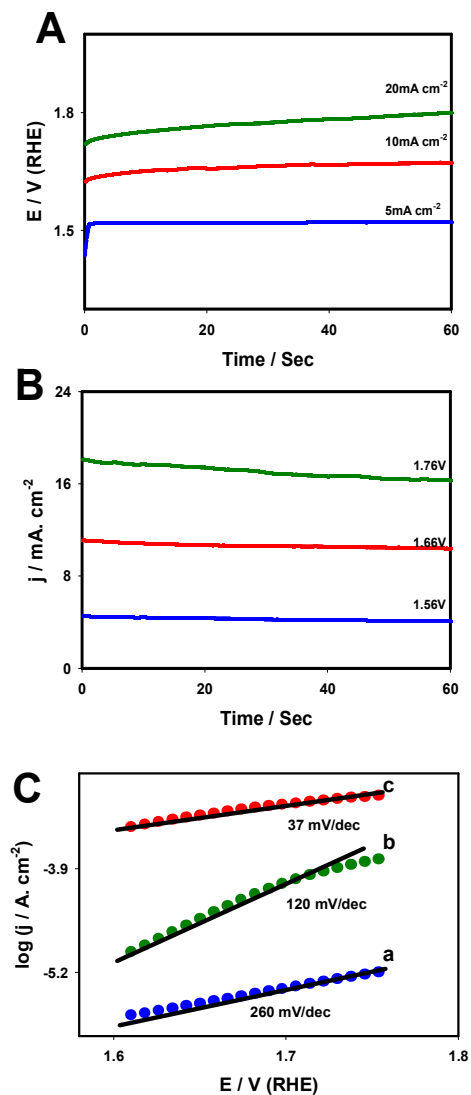
Fig. 5. (A) Chronopotentiometric curves of the Co QD/rGO nanocomposite electrode under high current densities of 5, 10, and 20 mA cm^{-2} in 0.1M KOH. (B) Amperometric response of the Co QD/rGO nanocomposite electrode under applied potentials of 1.56, 1.66 and 1.76V in 0.1M KOH. (C) Tafel plots of the rGO (a), Co (b) and Co QD/rGO nanocomposite electrodes (c).

smaller than that of RuO$_2$,[21] Pt/C,[21] and IrO$_2$,[28] signifying more efficient electron transfer in the Co QD/rGO nanocomposite for OER in comparison with these state-of-the-art electrocatalysts. The overpotential (η) of the Co QD/rGO nanocomposite electrode at 10.0 mA cm^{-2} was calculated to be

0.37 V, which is comparable with most of the advanced electrocatalysts listed in Table 2, but much lower than Pt/C (0.55 V), in a good agreement with the LSV results shown in Fig. 3. The actual loading and specific mass activities of electrocatalysts are vital to their practical applications. To further assess the OER catalytic activity of the Co QD/rGO nanocomposite, its mass activity and TOF at j = 10 mA cm^{-2} were calculated. The measured mass activity of the Co QD/rGO nanocomposite was 1250 A g^{-1}, which is significantly higher than the available data of the electrocatalysts listed in Table 2. The intrinsic catalytic activity of the Co QD/rGO nanocomposite was also characterized by TOF based on the assumption that every Co atom was catalytically active. The Co QD/rGO nanocomposite catalyst exhibited a much higher TOF (0.181 s^{-1}) when compared with the most of the recently developed electrocatalysts listed in Table 2. The high catalytic activity of the Co QD/rGO nanocomposite catalyst might be attributed to the small size of the Co QDs and their high dispersion and density, in conjunction with the electronic coupling effect of the Co QD and rGO sheets, which may provide vast highly active sites to accelerate the OER process. Moreover, surface resident Co QDs in basic solution might also provide abundant active sites for facilitating the adsorption of hydroxide ions on the electrode surface, which could play a critical role in enhancing the OER activity.

Table 2. A list of the compared recent electrocatalysts for OER in alkaline solution.

Catalyst	Mass activity (A g^{-1})	η (V)	Tafel slope (mV dec^{-1})	TOF (s^{-1})	[Ref]
NG-CoSe$_2$	60	0.36	40	0.035	21
Au@Co$_3$O$_4$	10	0.31	60	-	26
NiCoFeO	-	0.47	50	-	27
N-CG–CoO	-	0.34	71	-	17
IrO$_2$	20^a	0.30^a	49	0.008	28
RuO$_2$	50	0.36	69	0.017	21
Pt/C	10	0.55	127	0.005	21
ZnCo-LDH	-	0.46	85	0.880	29
Co$_3$O$_4$/GR	-	0.37	67	-	8
NiCo$_2$S$_4$@N/S-rGO	-	0.47	51	-	30
NiCo(OH)$_2$	-	0.30	54	0.014	31
Co QD/rGO	**1250**	**0.37**	**37**	**0.181**	**This work**

^{a} The overpotential was calculated at 5 mA cm^{-2}.

Besides the catalytic activity, stability is another key parameter toward the development of cost effective catalysts for OER. To examine the stability of the Co QD/rGO nanocomposite electrode, long-term amperometric i vs t measurements were performed by applying an electrode potential (E$_{app}$) of 1.66 V in 0.1 M KOH under an Ar-atmosphere for 40,000 s. For comparison, the stability of the
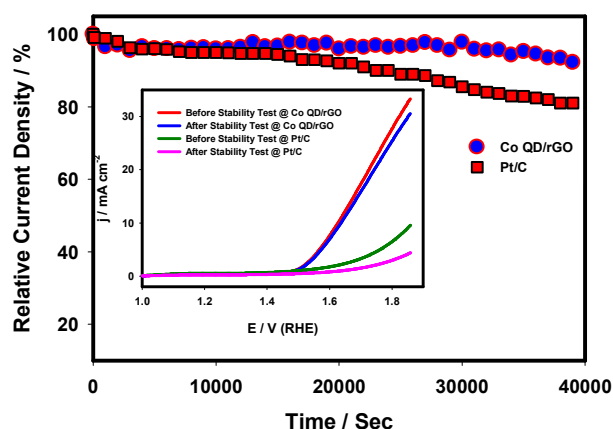
Fig. 6. Stability test of the Co QD/rGO nanocomposite and Pt/C electrodes for OER at E_{app} = 1.66 V in 0.1M KOH. Inset: LSV curves for OER at Co QD/rGO nanocomposite and Pt/C electrodes prior to and following the stability test.

start-of-the-art Pt/C was also tested. As shown in Fig. 6, the current density decay at the Co QD/rGO nanocomposite electrode was less than 9% over the test period, which was much slower than that at the Pt/C electrocatalyst (~18% loss of activity). LSV curves of the Co QD/rGO nanocomposite and Pt/C electrodes were also recorded prior to and following the stability tests in 0.1 M KOH. As shown in the inset of Fig. 6, no notable changes in the onset potential and current density were observed for the Co QD/rGO nanocomposite electrode; however, a significant decrease of current density toward OER was seen at the Pt/C electrode, further confirming that the Co QD/rGO nanocomposite electrode was highly suitable for OER. Finally, the reproducibility of the Co QD/rGO electrocatalyst was investigated. Three Co QD/rGO nanocomposite modified GC electrodes were prepared and investigated for OER activity under identical experimental conditions. The resulting relative standard deviation (RSD) was calculated at j = 10mA cm^{-2} to be 1.32%, which validates an acceptable reproducibility of the Co QD/rGO nanocomposite electrode for OER in 0.1 M KOH.

4. Conclusions

In summary, a novel Co QD/rGO nanocomposite, comprised of an excellent platform for the promotion of OER activity through the presence of abundant catalytically active sites and enhanced conductivity, was successfully synthesized using a facile in situ chemical reduction strategy. As a result, this economical nanocomposite electrocatalyst yielded an exceptional OER mass activity of 1250 A g^{-1} with a low η of 0.37 V at a current density of 10 mA cm^{-2}, and small Tafel slope of 37 mV dec^{-1} in 0.1 M KOH. The Co QD/rGO nanocomposite electrode exhibited ~10 times higher catalytic activities in comparison to GC electrode modified with Co nanoparticles. Moreover, it possessed lower overpotential, higher catalytic activity and higher stability than the state-of-the-art Pt/C

catalyst. The present work not only provides a facile and simple strategy for the preparation of the Co QD/rGO nanocomposite, but concurrently verifies it as an outstanding platform for the optimization of OER. This study serves as a strong prerequisite for the design of effective OER electrocatalysts, through the suitable chemical and electrical coupling of functional materials, toward a viable hydrogen economy.

Acknowledgements

Notes and references

‡ **Electronic Supplementary Information available:** XRD and FT-IR measurements for the Co QD/rGO nanocomposite; the plot of onset potentials (E_{onset}) and oxidation potentials at 5 mA cm^{-2} of different eletrocatalysts; chronopotentiometric and amperometric curves of the GC electrode modified with Co nanoparticles recorded under various current densities and electrode potentials in 0.1M KOH.

Notes: The authors declare no competing financial interest.

1   C. G. Morales-Guio, L. -A. Ster and X. Hu, *Chem. Soc. Rev*. 2014, **43**, 6555.
2   B. Li, X. Ge, F. W. Thomas Goh, T. S. Andy Hor, D. Geng, G. Du, Z. Liu, J. Zhang, X. Liu, Y. Zong, *Nanoscale*, 2015, **7**, 1830.
3   X. Long, J. Li, S. Xiao, K. Yan, Z. Wang, H. Chen and S. A. Yang, *Angew. Chem. Int. Ed*. 2014, **53**, 1.
4   J. Suntivich, K. J. May, H. A. Gasteiger, J. B. Goodenough and Y. A. Shao-Horn, *Science* 2011, **33**, 1383.
5   A. Fortunelli, W. A. Goddard III, L. Sementa and G. Barcaro, *Nanoscale*, 2015, **7**, 4514.
6   L. Wu, Q. Li, C. H. Wu, H. Zhu, A. Mendoza-Garcia, B. Shen, J. Guo, S. Sun, *J. Am. Chem. Soc*. 2015, **137**, 7071.
7   Y. Su, Y. Zhu, H. Jiang, J. Shen, X. Yang, W. Zou, J. Chen and C. Li, *Nanoscale*, 2014, **6**, 15080.
8   B. H. R.Suryanto, X. Lu and C. Zhao, *J. Mater. Chem. A* 2013, **1**, 12726.
9   Y. Q. Fan, H. B. Shao, J. M. Wang, L. Liu, J. Q. Zhang and C. N. Cao, *Chem. Commun*. 2011, **47**, 3469.
10 F. Jiao and H. Frei, *Angew. Chem., Int. Ed*. 2009, **48**, 1841.
11 Z. Zhuang, W. Sheng and Y. Yan, *Adv. Mater*. 2014, **26**, 3950.
12 K. S. Mali, J. Greenwood, J. Adisoejoso, R. Phillipson and S. De Feyter, *Nanoscale*, 2015, **7**, 1566.
13 Y. Zhu, X. Ji, C. Pan, Q. Sun, W. Song, L. Fang, Q. Chen, C. E. Banks, *Energy Environ. Sci*. 2013, **6**, 3665.
14 D. A. C. Brownson, D. K. Kampouris and C. E. Banks, *Chem. Soc. Rev*. 2012, **41**, 6944.
15 A. Chen and S. Chatterjee, *Chem. Soc. Rev*. 2013, **42**, 5425.
16 F. Li, X. Jiang, J. Zhao and S. Zhang, *Nano Energy* 2015, 16, 488.
17 S. Mao, Z. Wen, T. Huang, Y. Hou and J. Chen, *Energy Environ. Sci*. 2014, **4**, 609.

18 M. Srivastava, M. E. Uddin, J. Singh, N. H. Kim and J. H. Lee, *J. Alloys Compd*. 2014, **590**, 266.

19 C. Peng, B. Chen, Y. Qin, S. Yang, C. Li, Y. Zuo, S. Liu and J. Yang, *ACS Nano* 2012, **6**, 1074.

20 H. Du, Q. Liu, N. Cheng, A. M. Asiri, X. Sun, C. M. Li, *J. Mater. Chem. A* 2014, **2**, 14812.

21 M-R. Gao, X. Cao, Q. Gao, Y.-F. Xu, Y-R. Zheng, J. Jiang and S.-H. Yu, *ACS Nano* 2014, **8**, 3970.

22 Y. Chen, Q. Wang, C. Zhu, P. Gao, Q. Ouyang, T. Wang, Y. Ma and C. Sun, *J. Mater. Chem*. 2012, **2**, 5924.

23 Y. Yao, C. Xu, J. Qin, F. Wei, M. Rao and S. Wang, *Ind. Eng. Chem. Res*. 2013, **5**, 17341.

24 Z. Fan, J. Yan, L. Zhi, Q. Zhang, T. Wei, J. Feng, M. Zhang, W. Qian and F. Wei, *Adv. Mater*. 2010, **22**, 3723.

25 Wagner, C. D.; Riggs, W. M.; Davis, L. E.; Moulder, J. F.; G. E. Muilenberg, Handbook of X-ray Photelectron Spectroscopy, Perkin-Elmer Corporation, 1979, P. 38.

26 Z. Zhuang, W. Sheng and Y. Yan, *Adv. Mater*. 2014, **26**, 3950.

27 Y. Cheng, C. Liu, H.-M. Cheng and S. P. Jiang, *ACS Appl. Mater. Interfaces* 2014, **6**, 10089.

28 L. Trotochaud, J. K. Ranney, K. N. Williams and S. W. Boettcher, *J. Am. Chem. Soc*. 2012, **134**, 17253.

29 Y. Li, L. Zhang, X. Xiang, D. Yan and F. Li, *J. Mater. Chem. A* 2014, **2**, 13250.

30 Q. Liu, J. Jin and J. Zhang, *ACS Appl. Mater. Interfaces* 2013, **5**, 5002.

31 L. Wang, C. Lin, D. Huang, F. Zhang, M. Wang, J. Jin, *ACS Appl. Mater. Interfaces* 2014, **6**, 10172.

Nanoscale Accepted Manuscript